Inorganic Chemistry

Article

pubs.acs.org/IC

Electronic Structure of Nickel(II) and Zinc(II) Borohydrides from Spectroscopic Measurements and Computational Modeling

Patrick J. Desrochers,*[,†] Christopher A. Sutton,[†] Micah L. Abrams,[‡] Shengfa Ye,[§] Frank Neese,[§] Joshua Telser,*[,⊥] Andrew Ozarowski,[∥] and J. Krzystek[∥]

[†]Department of Chemistry, University of Central Arkansas, Conway, Arkansas 72035, United States

[‡]EOIR Technologies, Lorton, Virginia 22079, United States

[§]Max-Planck Institute for Bioinorganic Chemistry, Stiftstrasse 34-36, D-45470 Mülheim an der Ruhr, Germany

[⊥]Department of Biological, Chemical and Physical Sciences, Roosevelt University, Chicago, Illinois 60605, United States

[∥]National High Magnetic Field Laboratory, Florida State University, Tallahassee, Florida 32310, United States

Supporting Information

ABSTRACT: The previously reported Ni(II) complex, Tp*Ni(κ^3-BH_4) (Tp* = hydrotris(3,5-dimethylpyrazolyl)-borate anion), which has an S = 1 spin ground state, was studied by high-frequency and -field electron paramagnetic resonance (HFEPR) spectroscopy as a solid powder at low temperature, by UV−vis−NIR spectroscopy in the solid state and in solution at room temperature, and by paramagnetic ^{11}B NMR. HFEPR provided its spin Hamiltonian parameters: D = 1.91(1) cm^{-1}, E = 0.285(8) cm^{-1}, $\mathbf{g}$ = [2.170(4), 2.161(3), 2.133(3)]. Similar, but not identical parameters were obtained for its borodeuteride analogue. The previously unreported complex, Tp*Zn(κ^2-BH_4), was prepared, and IR and NMR spectroscopy allowed its comparison with analogous closed shell borohydride complexes. Ligand-field theory was used to model the electronic transitions in the Ni(II) complex successfully, although it was less successful at reproducing the zero-field splitting (zfs) parameters. Advanced computational methods, both density functional theory (DFT) and ab initio wave function based approaches, were applied to these Tp*MBH_4 complexes to better understand the interaction between these metals and borohydride ion. DFT successfully reproduced bonding geometries and vibrational behavior of the complexes, although it was less successful for the spin Hamiltonian parameters of the open shell Ni(II) complex. These were instead best described using ab initio methods. The origin of the zfs in Tp*Ni(κ^3-BH_4) is described and shows that the relatively small magnitude of D results from several spin−orbit coupling (SOC) interactions of large magnitude, but with opposite sign. Spin−spin coupling (SSC) is also shown to be significant, a point that is not always appreciated in transition metal complexes. Overall, a picture of bonding and electronic structure in open and closed shell late transition metal borohydrides is provided, which has implications for the use of these complexes in catalysis and hydrogen storage.

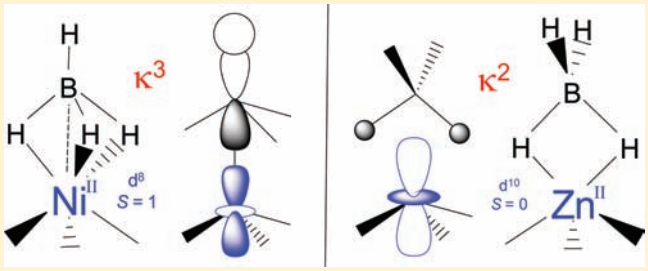

INTRODUCTION

Metal borohydrides are established reducing agents in organic reactions. Reviews by Marks and Kolb[1] and by Ganem and Osby[2] outline both the transition metal-catalyzed borohydride reductions of organic molecules and the structural features of metal-borohydrides. Over the past decade, interest in these materials has further evolved with borohydrides attracting attention as potential materials for solid state hydrogen storage applications.[3,4] This interest encompasses related hydrogen-rich species such as aluminohydrides ($MAlH_4$) and amineborane (NH_3BH_3),[5] a compound with the highest gravimetric hydrogen content (19.7%) of any of the leading materials for solid phase hydrogen storage. In some cases, nickel and other transition metals can play a role in the catalytic decomposition of these solid phase hydrides.[6]

Nickel exhibits rich and varied borohydride chemistry. This includes species in which the nickel ion has been reduced by BH_4^-, as well as several instances where borohydride persists as an intact chelate. Raney nickel, an active industrial hydrogenation catalyst that contains nickel(0), is generally prepared via the reduction of simple nickel(II) salts (where the metal ion is effectively unprotected) using borohydride or aluminohydride.[7] One of the earliest reported discrete nickel(II)-borohydride complexes, possessing a N_4Ni(κ^2-BH_4) coordination sphere,[8] established the ability of nitrogen-donor chelates to retard reduction of nickel(II) by borohydride.[9,10] This observation was most recently confirmed by the report of a structurally characterized BH_4-bridged nickel(II)-nickel(II) dimer, where the dinuclear metal center was supported with a hexaaza-dithiophenolate chelate.[11] In contrast, in soft phosphine ligand environments, nickel(II) is readily reduced,

Received: August 15, 2011
Published: February 15, 2012

 © 2012 American Chemical Society dx.doi.org/10.1021/ic201775c | Inorg. Chem. 2012, 51, 2793−2805

yielding phosphine-nickel(I)-borohydrides.[12,13] The subject of this present report is a complex with a $N_3Ni(\kappa^3\text{-}BH_4)$ coordination sphere, Tp^*NiBH_4, where Tp^{*-} is hydrotris(3,5-dimethylpyrazolyl)borate (Figure 1),[14] which was isolated as a moisture and air stable green solid.[15]

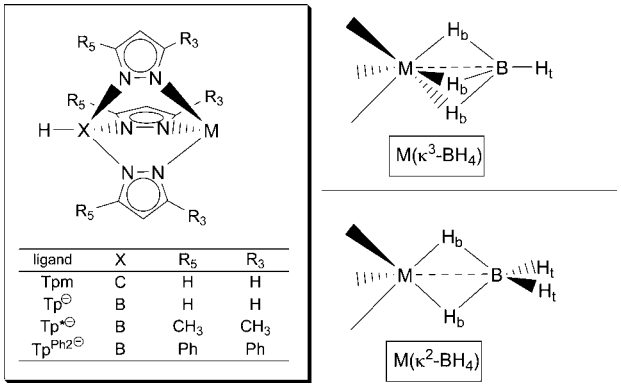

Figure 1. Trispyrazolyl ligand abbreviations and metal-borohydride coordination modes discussed in this work. Kappa notation refers to the number of coordinated hydrogen atoms from the borohydride ligand.

Tp^*NiBH_4 is a paradigm for stable transition metal borohydrides for several reasons. First, this system represents the most extensively characterized paramagnetic transition metal borohydride to date. Despite being the subject of several reviews,[1,16] the nature of metal-borohydride bonding remains a topic of great interest, and modern computational and spectroscopic methods such as those described here can add to this understanding. Increasingly more accurate theoretical and experimental descriptions should improve borohydride utility both as a common reagent and as a potential solid phase hydrogen storage matrix. Second, it is useful to determine the role an appropriately coordinated metal ion can play in controlling the reactivity of borohydride ion. Most recently, Mehn et al. reported the use of ancillary ligands, Tp^{Ph2-} and $PhB(CH_2PPh_2)_3^-$, to yield respectively, high-spin and low-spin iron(II) borohydrides.[17] Their report included a bonding model for the $Fe(\kappa^3\text{-}BH_4)$ framework in which π interactions between iron(II) and the ancillary chelates determined the electron spin state and frontier orbital structure in these systems. It was proposed that the κ^3-borohydride could be described as a *tetradentate* ligand (i.e., $\kappa^4\text{-}BH_4$;[8] see Figure 1) involving covalent interactions with the three bridging hydrides *and* the boron atom.[17]

Herein we report complementary spectroscopic measurements and theoretical descriptions of Tp^*NiBH_4 to develop a self-consistent description of the bonding interaction between borohydride and nickel(II) and address the stability of this complex. High-frequency and -field EPR (HFEPR, defined here as frequencies above ~95 GHz and magnetic fields above ~3 T) and near-infrared (NIR) electronic spectroscopic measurements on Tp^*NiBH_4 were recorded. Supported by these experiments, computational models should establish a self-consistent theoretical model for the bonding in this complex. Classical ligand-field theory (LFT) models were able to explain the electronic absorption spectra of the nickel complex, but were not successful in modeling the spin Hamiltonian parameters obtained from HFEPR. In parallel, density functional theory (DFT) was also applied here. The utility of DFT was first tested by predicting the geometry of a closed-shell Tp^*ZnBH_4 complex. Experimental validation is provided by the preparation of $Tp^*Zn(\kappa^2\text{-}BH_4)$, here for the first time, whose spectroscopic characteristics mirror those of its structurally characterized congener, $Tp^*Cd(\kappa^2\text{-}BH_4)$.[18] While DFT gives excellent predictions of structural and vibrational properties of both Zn(II) and Ni(II) complexes, a higher level of theory invoking explicit electron correlations and multi-reference wave functions of low lying excited states was essential to predict electronic properties of the open-shell complex, high spin Tp^*NiBH_4. The present work was undertaken to describe the extent of covalent interaction within the $Ni(\kappa^3\text{-}BH_4)$ framework and discuss its role in the observed stability and reactivity of the BH_4^- group. It is hoped that such models will improve the utility and understanding of stable transition metal borohydrides and thereby foster their greater applications including hydrogen-based energy sources and metal-catalyzed reductions.

EXPERIMENTAL SECTION

General Procedures. Solvents from Fisher Scientific and reagents from Sigma Aldrich were used as received. NMR spectra were recorded using a JEOL ECX-300 spectrometer and infrared spectra were recorded using a Thermo Nicolet FTIR 100 spectrophotometer. Solution phase IR spectra were recorded for 50 mM solutions and utilized a cell with sodium chloride windows and a path length of 0.5 mm.

Synthesis of $Tp^*M(\kappa^2\text{-}BH_4)$, M = Ni, Zn. The ligand salt, KTp^* was prepared according to literature methods.[19] Tp^*NiBH_4 was prepared from the reaction of Tp^*NiNO_3 and $NaBH_4$ in acetonitrile according to methods previously described.[15] Infrared spectra of Tp^*NiBH_4 were recorded as part of this previous study, but were not presented, and are thus shown here for the first time. Tp^*ZnBH_4 was prepared from Tp^*ZnCl,[20,21] following a procedure developed in this laboratory for nickel(II).[22] In a two-phase reaction, Tp^*ZnCl (120 mg, 0.30 mmol) dissolved in 5 mL of dichloromethane was stirred vigorously with solid $NaBH_4$ (500 mg). The reaction was monitored periodically by ^{11}B NMR spectroscopy; over time the conversion of Tp^*ZnCl to Tp^*ZnBH_4 was noted by the appearance of the sharp new quintet resonance at $\delta = -50.20$ ppm of zinc-coordinated borohydride. Progress was deemed complete when the relative integral of this quintet equaled that of the Tp*-boron signal at $\delta = -10.66$ ppm. After 3 h, undissolved solids were filtered, and the clear colorless filtrate was reduced in volume to about one-fourth under a dry nitrogen stream. The addition of hexanes to this solution induced precipitation of a pearlescent white solid. Yield 80 mg. The deuterated form is readily prepared by the same method using sodium borodeuteride (Aldrich, 96 atom % D). Anal. for $C_{15}H_{26}B_2N_6Zn$, Expt (Calc): C, 47.82 (47.73); H, 6.67 (6.94); N, 22.34 (22.27). IR (KBr): ν(B-H) 2529 cm^{-1} (H-B, Tp*), 2442 cm^{-1} and 2405 cm^{-1} (H_t-B, assym. and sym.), 2113 cm^{-1} (H_b-B). ^1H NMR (CD_2Cl_2; δ residual H at 5.32 ppm) $\delta = 0.68$ ppm (4 H, 1:1:1:1 quartet, $J_{BH} = 83$ Hz, BH_4), 2.31 ppm (9 H, singlet, 3-position-CH_3), 2.36 ppm (9 H, singlet, 5-position-CH_3), 5.79 ppm (3 H, singlet, 4-H pyrazole ring). ^{13}C NMR (CD_2Cl_2; δ at 53.8 ppm) 12.54, 12.94 ppm (-CH_3), 105.64 ppm (ring 4-C), 145.74, 150.04 ppm (ring 3,5-C). ^{11}B NMR (CD_2Cl_2; δ vs $[NBu_4]BF_4$ at −2.50 ppm) $\delta = -10.66$ ppm (broad doublet, $J_{B\text{-}H} = 110$ Hz, H-B of Tp*), −50.20 ppm (quintet, 1:4:6:4:1, $J_{BH} = 83$ Hz, BH_4).

Electronic Absorption Spectroscopy. Electronic spectra were recorded using a Jasco 570 UV−vis−NIR (25,000 to 4,000 cm^{-1}) spectrophotometer with samples in 1 cm Suprasil cuvettes at ambient temperature. Near IR region (10,000−4,000 cm^{-1}) spectra were recorded using CD_2Cl_2 as solvent, to minimize interference from ν(C-H) harmonics. Comparison between NIR spectra for neat CD_2Cl_2 and Tp^*NiBH_4 in solution clearly distinguished between the sharp vibrational lines from solvent and the broad electronic transitions arising from nickel(II). In addition, diffuse reflectance spectra were recorded from 25,000−5,000 cm^{-1} at ambient temperature for Tp^*NiBH_4 mixed with MgO powder, with the MgO spectrum subtracted as a

dx.doi.org/10.1021/ic201775c | Inorg. Chem. 2012, 51, 2793−2805

background correction. Band positions in the solid samples were effectively the same as for the solution phase measurement, indicating similar nickel(II) electronic environments in both matrixes (Supporting Information, Figure S1).

HFEPR Spectroscopy. Spectra were recorded using primarily the Millimeter and Submillimeter Wave Facility at NHMFL,[23] with some experiments performed at the EMR Facility.[24] The former experimental setup employs tunable frequencies in the 50 GHz−1.2 THz range, of which 150−700 GHz were used in this work, and the resistive "Keck" magnet, enabling 0−25 T field sweeps. Detection was provided with an InSb hotelectron bolometer (QMC Ltd., Cardiff, U.K.). Modulation for detection purposes was provided alternatively by chopping the subterahertz wave beam ("optical modulation") or by modulating the magnetic field. A Stanford Research Systems SR830 lock-in amplifier converted the modulated signal to direct current (DC) voltage. Parameters occurring in the standard spin Hamiltonian for $S = 1$:[25]

$$\mathcal{H} = \beta \mathbf{B}\cdot\mathbf{g}\cdot S + D(S_z^2 - S(S+1)/3) + E(S_x^2 - S_y^2), \quad (1)$$

were fit to the 2-D field/frequency maps, as described elsewhere.[26]

COMPUTATIONAL METHODS

Ligand-Field Theory (LFT). LFT calculations were made using the locally written program DDN (available from J. Telser) and the program Ligfield, written by J. Bendix.[27] We also employed the values that Bendix et al. have determined for single electron spin−orbit coupling (SOC) parameters, ζ_{nd}, for gaseous transition metal ions. For Ni^{2+}, their free-ion value is $\zeta_{nd} = 668(9)$ cm^{-1}.[27] Values ranging from 630−648 cm^{-1} are found in other sources.[25,28,29] Values for the interelectronic repulsion (Racah) parameters $B = 1042$ cm^{-1} and $C = 4604$ cm^{-1} are also from the Copenhagen group,[30] which can also be found elsewhere.[28]

Quantum Chemistry Theory. All calculations in this work were performed with the ORCA program package.[31] Geometry optimizations and vibrational frequency calculations for Tp*NiBH$_4$ and Tp*ZnBH$_4$ were carried out with the BP86[32−34] density functional in conjunction with the scalar relativistic zeroth-order regular approximation (ZORA).[35−37] The ZORA-TZVP basis sets[38,39] were employed for all elements. The RI approximation[40] was used to speed up the calculation with the auxiliary basis sets TZV/J.[41,42]

Density functional theory (DFT) calculations of the zfs parameters of Tp*NiBH$_4$ were conducted at the ZORA/BP86[32−37] level of theory using the ZORA-TZV(2d,2p) basis set[38,39] for all atoms. The spin−spin coupling (SSC) contribution to the zfs was calculated on the basis of a single ground state Slater determinant, such as Kohn−Sham determinant, using the following equation:[43]

$$D_{kl}^{SSC} = \frac{g_e^2}{4}\frac{\alpha^2}{S(2S-1)}\sum_{\mu\nu}\sum_{\kappa\tau}\{P_{\mu\nu}^{\alpha-\beta}P_{\kappa\tau}^{\alpha-\beta} - P_{\mu\kappa}^{\alpha-\beta}P_{\nu\tau}^{\alpha-\beta}\}\langle\mu\nu|r_{12}^{-5}\{3r_{12,k}r_{12,l} - \delta_{kl}r_{12}\}|\kappa\tau\rangle \quad (2)$$

in which the spin density matrix $\mathbf{P}^{\alpha-\beta}$ was obtained on the basis of the spin-unrestricted natural orbital (UNO) determinant.[44] The spin−orbit coupling (SOC) part of the zfs was estimated by the coupled-perturbed approach.[45] In the evaluation of SOC integrals, the SOC operator was represented by the spin−orbit mean field (SOMF) approximation[46,47] in the implementation described elsewhere.[48]

Quasi-degenerate perturbation theory (QDPT)[49] was used to verify the DFT results as described previously for the related d^2 systems.[50] The computational method is based on ab initio wave function based approaches such as complete active space self-consistent field (CASSCF), and the recently implemented second-order N-electron valence perturbation theory (NEVPT2).[51,52] In all ab initio calculations the ZORA approximation[35−37] was employed along with the ZORA-TZV(2d,2p) basis set[38,39] for all elements. According to our previous experience, the simplest possible active space was chosen in which eight electrons were distributed into the five Ni 3d-based molecular orbitals (CAS(8,5)). In state-averaged CASSCF (SA-CASSCF) calculations the orbitals were optimized for the average of 10 triplet and 15 singlet roots. Diagonalization of the SOC matrix, which is constructed in the basis of the state-averaged CASSCF (SA-CASSCF) roots, yields the energies of the spin−orbit split components of the electronic ground and the d-d excited states. Thus, this treatment amounts to an ab initio realization of ligand-field theory that takes differential orbital covalency into account. The SSC contributions were estimated using the Breit-Pauli spin−spin Hamiltonian in conjunction with first-order perturbation theory.[53] In NEVPT2 calculations, only the perturbed energies enter the QDPT procedure while the wave function remained at the SA-CASSCF level.

RESULTS AND DISCUSSION

We begin by describing the new results obtained for the previously characterized Tp*NiBH$_4$ complex. These include solid state HFEPR and electronic absorption studies. We then apply LFT and quantum chemical calculation to describe the electronic structure of the complex. The new Tp*ZnBH$_4$ complex is then described, including synthesis, reactivity, and computational studies.

HFEPR Results for Tp*NiBH$_4$ and Tp*NiBD$_4$. Solid polycrystalline Tp*NiBH$_4$ and Tp*NiBD$_4$ produce low-temperature (5−40 K) HFEPR spectra that can be interpreted as triplet powder-patterns.[54] HFEPR spectra of the two isotopologues are shown together in Supporting Information, Figure S2. An example of such a spectrum for Tp*NiBH$_4$ is shown in Figure 2 (black trace) together with two simulations:

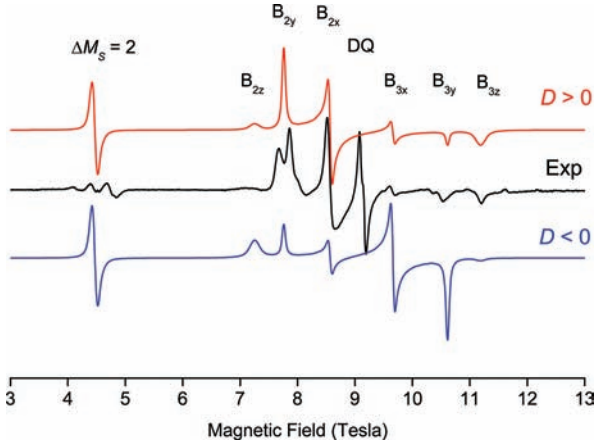

Figure 2. HFEPR spectrum of solid Tp*NiBH$_4$ at 281.56 GHz and 10 K. The black trace is experiment while the colored lines were simulated using the following spin-Hamiltonian parameters: $S = 1$, $|D| = 2.0$ cm^{-1}, $|E| = 0.3$ cm^{-1}, $g_x = 2.19$, $g_{y,z} = 2.18$. The red trace is a simulated spectrum using positive zfs parameters while the blue trace was simulated with negative ones. Specific turning points in the recorded spectrum are labeled (DQ = double quantum; not simulated).

one assuming a positive value for the zfs parameters (red trace) and the other a negative value (blue trace). It is apparent that the zfs parameter D is positive (E is attributed the same sign as D by convention). A characteristic of the experimental spectrum is the low intensity of the so-called B_{min} feature, corresponding to an off-axis turning point of the $\Delta M_S = \pm 2$ transition, compared to the simulations. Some of us have previously observed this phenomenon in other studies of triplet spin species,[55] and we interpret it via the imperfect powder

dx.doi.org/10.1021/ic201775c | Inorg. Chem. 2012, 51, 2793−2805

distribution of the crystallites in the sample. Simulations show that B_{min} dominates the spectrum only if that distribution is truly random; in a partly aligned sample its intensity is greatly reduced. In addition, the oversized transmission-type probe used for these measurements allows for a varying ratio of $B_{1(rf)} \parallel B_0$, and nominally forbidden $B_{1x,y,z}$ canonical turning points corresponding to the same $\Delta M_S = \pm 2$ transition, show up in the spectra at about the same field position as B_{min}, as seen in Figure 2 (also observed before[55]). The intense isotropic double-quantum (DQ) transition characteristic for HS Ni(II) EPR spectra[56] is not simulated.

We have tried to simulate the repeatable doubling of the B_{2y} and B_{3y} turning points by assuming a noncolinearity of the **g** and zfs (**D**) tensors, by analogy to what has been done in the case of a low-symmetry $S = 2$ Mn(III) complex,[57] but were unable to reproduce this effect. This failure is not surprising given the almost isotropic **g** tensor in our case. Also, the relatively higher symmetry of Tp^*NiBH_4 does not offer an obvious justification for this phenomenon. As a working hypothesis, we thus assumed an existence of two triplet states with minimally different spin Hamiltonian parameters and chose not to replicate this doubling in simulated spectra, instead using averaged values of D and E.

The accuracy of the experimentally derived spin Hamiltonian parameters was improved by performing a tunable-frequency experiment on Tp^*NiBH_4. By varying the frequency over a wide range (ca. 150 to 550 GHz with an additional frequency of 95 GHz) a two-dimensional map of resonances as a function of frequency was collected and is shown in Figure 3 along with

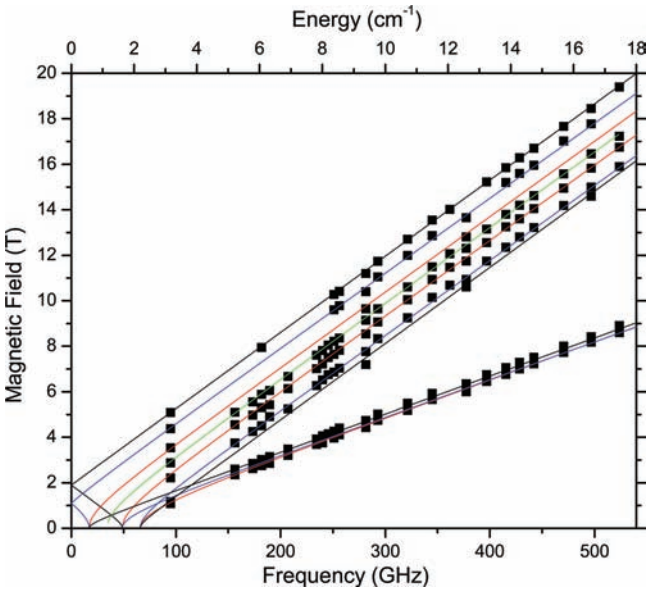

Figure 3. Resonance field vs frequency (quantum energy) dependence for Tp^*NiBH_4 at 4.5 K. Squares are experimental data; curves are simulated using parameters as in Table 1: red lines are $B_0 \parallel x$ turning points; blue lines are $B_0 \parallel y$ turning points; black lines are $B_0 \parallel z$ turning points; the green line is the double-quantum transition.

best-fits[26,58] using the Hamiltonian (Equation 1) parameters summarized in Table 1.

Solid polycrystalline Tp^*NiBD_4 produces low-temperature (5–40 K) HFEPR spectra that are analogous to those generated by Tp^*NiBH_4, consistent with what should be the same electronic structure for these isotopologues, although individual turning points are markedly broader in the deuteride (Supporting Information, Figure S2). Supporting Information, Figure S3 presents an example of a single-frequency HFEPR spectrum of Tp^*NiBD_4. Careful comparison with Figure 2 shows that the D parameter of the deuteride is not identical to that of the hydride, but is slightly larger. Supporting Information, Figure S3 also shows the doubling of the B_{2y} and B_{3y} turning points, accompanied by a corresponding doubling of the parallel (B_{2z} and B_{3z}) turning points, which shows that there also exist in Tp^*NiBD_4 two triplet spin states with slightly different spin Hamiltonian parameters. As for Tp^*NiBH_4, we ignore this doubling in our single-frequency simulations and use averaged parameters. The 2-D data set for Tp^*NiBD_4 is shown in Supporting Information, Figure S4, and the best-fit parameters are given in Table 1.

Differences in zero-field splitting parameters, of ~2% in D, between protio and deutero isotopologues are reported for $[V([H,D]_2O)_6]^{3+}$;[59,60] however, in these hexaaqua complexes, all of the ligands are directly affected by H/D substitution, whereas in Tp^*NiBH_4, the Tp^{*-} ligand is unaffected. We can only speculate that differences in crystal packing between the two isotopologues may be reflected in the differences in zfs.[61]

Electronic Absorption Spectroscopy of Tp^*NiBH_4. Earlier reports on the electronic absorption spectra for Tp^*NiBH_4 did not describe NIR transitions, and all spectra were recorded in solution, because of instrument limitations.[15] Here we report a previously unobserved, low energy d-to-d transition at 9,000 cm^{-1} for the compound in dichloromethane-d_2 solution and in the solid state by diffuse reflectance (all spectra shown in Supporting Information, Figure S1). These transitions for Tp^*NiBH_4 can collectively be assigned as the three symmetry forbidden but spin-allowed electronic transitions for nickel(II) in a pseudo-octahedral ligand field (see Table 2). If the symmetry is more realistically lowered from octahedral, but the 3-fold axis of the *fac*-N_3H_3 donor set maintained, then in both D_3 and C_{3v} point group symmetry, $^3A_2(F) \rightarrow {}^3A_2[{}^3T_1(F, P)]$ transitions are allowed with z-polarization and the various $^3A_2 \rightarrow {}^3E[{}^3T_1(F, P), {}^3T_2(F)]$ transitions are allowed with xy-polarization.

When fitted using LFT software, this pseudo-octahedral symmetry model yields reasonable values of $\Delta_o = 8650$ cm^{-1} and $B = 820$ cm^{-1}, as a consensus to the solution and solid state data. The *fac*-N_3H_3 donors impose a fairly weak ligand field on nickel(II) in this system, in contrast with much higher ligand fields seen in NiN_6 and tetragonal NiN_4X_2 (X = halide) donor environments (where $\Delta_o = 11{,}000–14{,}000$ cm^{-1}).[62–64] A weak ligand field for $Tp^RM(\kappa^3\text{-}BH_4)$ is further supported by the observation of a high-spin iron(II) center in $Tp^{Ph2}Fe(\kappa^3\text{-}BH_4)$.[17]

Several models are plausible for the ligand field imposed by $\kappa^3\text{-}BH_4^-$ coordinated to transition metal ions. One model considers the borohydride as a facially coordinated ligand, giving a formally C_{3v} six-coordinate nickel(II) center. This model is independently supported by the self-consistency of transition assignments in the electronic spectrum of the compound by assuming a pseudo octahedral model. Previously reported solid state X-ray absorption spectroscopy measurements on Tp^*NiBH_4 were also consistent with a centrosymmetric six-coordinate nickel(II) center, based on the lower intensity of the 1s to 3d near-edge electronic transition compared to the much higher intensity transition seen for pseudotetrahedral Tp^*NiCl under the same conditions.[15] Another model treats the $\kappa^3\text{-}BH_4^-$ ligand as a single donor, so that Tp^*NiBH_4 could be considered an extension of the pseudotetrahedral series of Tp^*NiX complexes studied previously.[65]

dx.doi.org/10.1021/ic201775c | Inorg. Chem. 2012, 51, 2793–2805

Table 1. Experimental Spin Hamiltonian ($S = 1$) Parameters for Tp*NiB(H,D)$_4$ with Values Calculated Using the Experimental Geometry and the Optimized Geometry (in Parentheses)

	D (cm^{-1})	$\|E\|$ (cm^{-1})	g_x	g_y	g_z
Tp*NiBH$_4$ expt.	+1.91(1)	0.285(8)	2.170(4)	2.161(3)	2.133(3)
calc., AOM[a]	−(0.74−0.88)	0.18−0.21			
calc., DFT[b]	+1.0 (+2.2)	0.02(0)	2.070 (2.072)	2.070 (2.072)	2.076 (2.077)
calc., CASSCF[b]	+1.5 (+2.6)	0.06(0)			
calc., NEVPT2[b]	+1.8 (+2.4)	0.05(0)			
Tp*NiBD$_4$ expt.	2.29(1)	0.29(2)	2.174(9)	2.153(9)	2.150(4)

[a]The zfs values are calculated by AOM using the six-coordinate model parameters given in Table 2, with (all values in cm^{-1}): C = 3600 ($C = 4.4B$) and ζ = 600−660 (~90−100% of the free-ion value); for comparison, use of the four-coordinate model and C = 3650 ($C = 4.4B$) and ζ = 660 gave D = 1.07, E = 0.28. Both models give $|E/D| = 0.24(1)$, in agreement with experiment ($|E/D| = 0.15$), but the magnitude of zfs is too small. [b]Details of these calculations are given in the Experimental Section. The contribution to D (all values in cm^{-1}) from SOC is D^{SOC} = +1.2, +1.5, respectively by CASSCF and NEVPT2 (see Supporting Information, Table S2); that from SSC is: D^{SSC} = +0.3 by both methods.

Table 2. Comparison of Experimental and Calculated Electronic Transition Energies (in cm^{-1}) for Tp*NiBH$_4$

assignment	calculated				experimental
$^3A_{2g}$(F) ground state	B3LYP/ 6−311++G**	CASSCF	NEVPT2	LFT,[a] [AOM], |AOM + SOC|	CH_2Cl_2 solution[b] [MgO reflectance]
→ $^3T_{2g}$(F)	12,100	7,660	11,260	8,650 [8,600−8,700] |8,300−9,100|	9,400 [9,100]
→ $^3T_{1g}$(F)	18,500	13,680	19,770	14,160 [13,900−14,300] |13,800−15,200|	13,700 [13,600]
→ ^1E_g(D)		17,730	15,710	13,525 [13,540] |13,040|	*c*
→ $^1T_{2g}$(D)		28,450	27,350	21,820 21,700−21,900 |21,300−21,900|	unobserved
→ $^3T_{1g}$(P)		27,890	29,420	24,085 [23,900−24,200] |23,900−24,600|	24,400 [24,000]

[a]Octahedral crystal field (all values in cm^{-1}) with B = 820, Dq = 865 (consensus values, fitting both solution and solid state spectra). AOM used B = 823, metrical parameters in Supporting Information, Table S1, and three equivalent pyrazole ligands with ε_σ(N) = 5700, and three equivalent hydrogen ligands with ε_σ(H) = 134. Ranges are given; symmetry is reduced by the two types of ligand and small, trigonal and rhombic distortions result. The AOM + SOC calculation adds spin−orbit coupling given by ζ = 600−660 (90%−100% of the free-ion value), which results in state mixing and partial allowedness of spin-forbidden transitions. Broader calculated bands result in this case compared to the AOM absent SOC. Similar results obtained using a four-coordinate model: B = 830, three equivalent pyrazole ligands with ε_σ(N) = 5800, and one borohydride ligand with $\varepsilon_\sigma(BH_4) = -50$. [b]$CD_2Cl_2$ solvent was used for NIR spectra. [c]A slight asymmetry of the $^3A_{2g} \rightarrow {}^3T_{1g}$(F) band toward higher energy may be observed in the experimental spectrum (Supporting Information, Figure S1), suggesting the presence of this spin forbidden transition and/or combined with a trigonal splitting of T_1(F) as AOM suggests.

A final model, as was postulated for Tp^{Ph2}Fe(BH$_4$),[17] is that the boron atom is also involved in bonding, giving κ^4-BH$_4^-$.[8] This model is discussed in detail in the quantum chemistry section below.

Modeling of Electronic Transitions in Tp*NiBH$_4$. Electronic transitions were modeled for Tp*NiBH$_4$ using both empirical (LFT) and computational (DFT) models. Two types of LFT models were used, one with crystal-field parameters as defined by Ballhausen[66] and one with the angular overlap model (AOM).[28,67] The crystal-field model assumed octahedral symmetry, but gave good agreement with the experimental data (Table 2). The AOM, where the actual symmetry of the complex is better modeled despite using idealized positions of the three H ligands, also gave good agreement. The metrical parameters used for the AOM, based on the crystal structure of Tp*NiBH$_4$, are given in Supporting Information, Table S1. The value for B = 823(6) cm^{-1} agrees exactly with the crystal-field model and is ~80% of the free-ion value.[28,30] More importantly, the bonding parameter for the pyrazole nitrogen ligands, ε_σ(N) = 5700(100) cm^{-1}, agrees quite well with the values determined for the same donors in the pseudotetrahedral Tp*NiX (X = Cl, Br, I) series studied previously (ε_σ = 5100−6100 cm^{-1}).[65] A study of HB(^{t}BuIm)$_3$NiBr, in which HB(^{t}BuIm)$_3$ is trisimidazolylhydroborate (i.e., a triscarbene analogue of trispyrazole), suggested ε_σ(C) = 6600 cm^{-1}; a carbene would be expected to be a stronger donor than pyrazole N.[68]

The bonding parameters for the H donors of κ^3-BH$_4^-$ were found to be quite small: ε_σ(H) = 134(1) cm^{-1}. If these individual values are simply summed, then they correspond to a single ligand with $\varepsilon_\sigma \approx 400$ cm^{-1}. We have no reference data for such a system, as these are not hydrido ligands; however, the overall weak ligand field is consistent with high spin ground states for Tp^{R}MBH$_4$ complexes (M = Ni(II), Fe(II)). Given the relatively few electronic transitions observed, the use of a minimal parameter space (i.e., all N- and H-donors equivalent and all with only σ-bonding) is preferred. The possibility of π-bonding by the Tp*$^-$ N-donors was explored; however, this had little effect, causing only a corresponding slight increase in

dx.doi.org/10.1021/ic201775c | Inorg. Chem. 2012, 51, 2793−2805

Table 3. Comparison of Measured and Geometry Optimized Bond Distances (Å) for Metal-Borohydrides in *fac*-tris(pyrazolyl) Donor Environments[a]

	Tpm*Li(κ^3-BH_4)		Tp^{Ph2}Fe(κ^3-BH_4)		Tp*Ni(κ^3-BH_4)		Tp*Zn(κ^2-BH_4)	Tp*Cd(κ^2-BH_4)	
	expt.[92]	calc.	expt.[17]	calc.[17]	expt.[15]	calc.	calc.	expt.[18]	calc.
⟨M-N⟩	2.056	2.172	2.106	2.100	2.001(4)	2.014	2.071	2.255(3)	2.293
M-B	2.223(7)	2.134	2.084(4)	2.051	2.048(5)	1.985	2.211	2.423(5)	2.399
⟨M-H_b⟩	2.06−2.12	2.045	1.99(2)	1.968	1.909 (avg.) 1.87−1.94	1.878	1.854	1.97−2.13	2.038
⟨B-H_b⟩[b]	0.79	1.244	1.16(2)	1.263	1.166 (avg.) 1.13−1.18	1.269	1.263	1.14−1.17	1.269
⟨B-H_t⟩[b]	0.79	1.214	0.98(5)	1.201	0.875	1.198	1.210	1.05−1.07	1.209

[a]Ligand structures and corresponding abbreviations are summarized in Figure 1. [b]For comparison, B-H distances in $LiBH_4$ ranged from 1.04(2)−1.28(1) Å (293 K).[88,93] The optimized B-H bond distance in gas-phase BH_4^- is 1.252 Å. Covalent radii, Å (CN = 6): Li^+ 0.90, Ni^{2+} 0.83, Fe^{2+} (high spin) 0.92, Zn^{2+} 0.89, Cd^{2+} 1.09. Ionic radii, Å (CN = 6): Li^+ 0.76, Fe^{2+} (high spin) 0.78, Ni^{2+} 0.69, Zn^{2+} 0.74, Cd^{2+} 0.95.[94]

ε_σ for the H ligands. Other LFT studies on scorpionate complexes employed only σ-bonding for trispyrazolyl ligands on Co(II) (Tp^RCoL[69,70]) and trisimidazolyl ligands on Ni(II).[68] On the other hand, π-donation by Tp^- to Cr(III) was proposed in a detailed optical spectroscopic and AOM analysis of $[Tp_2Cr]^+$.[71] Therefore, we cannot exclude π-bonding, and there may be evidence for it in the quantum chemistry results described below.

Another approach was to use the AOM with only four ligands, the Tp* N-donors as above, but with a single ligand along the z axis representing the κ^3-BH_4^-. This model essentially converged to the one described above. Best fit values were as follows: B = 830(10) cm^{-1}, ε_σ(N) = 5800(100) cm^{-1}, and ε_σ(H) = −50(100) cm^{-1}. A final model was to include the B atom as a ligand (located along the +z axis). This led to the following fit parameters for the electronic spectra: B = 830 cm^{-1}, ε_σ(N) = 5630 cm^{-1}, ε_σ(H) = 310 cm^{-1}, ε_σ(B) = −255 cm^{-1}. Negative values for ε_σ(H) should not be given too much significance; the point is simply that bonding to the borohydride is weak, and might even act as an electron acceptor from nickel via boron. This supports the computational results given below.

Given the reasonable fit to electronic transitions provided by the AOM in the absence of spin−orbit coupling (SOC), we then included this effect to provide a calculated zfs value to compare with experimental results from HFEPR (see Table 1). Unfortunately, the calculated D value is too small in magnitude (maximum of ∼1 cm^{-1}), even when ζ values that are ∼90−100% of the free-ion value (668 cm^{-1})[27] are employed, noting that a Racah B value ∼80% of the free-ion value was appropriate.[72] The AOM calculations do yield a significant rhombic component for the zfs: $|E/D| \approx 0.24(1)$, which is in good agreement with the experimental value (0.21). This rhombicity arises in both the six- and the four-coordinate models from use of the crystallographically based values for θ (Supporting Information, Table S1).[73]

The shortcomings of the AOM calculation may be due to several factors, in addition to the inherent difficulty of using only the metal ion $3d^8$ basis set without ligand contributions. First, the experimental D value is quite small in magnitude (1.91 cm^{-1}), so that a difference of only ∼1 cm^{-1} from the AOM calculation translates into an error of ∼100%. Second, the AOM used in this case is a very crude approximation, particularly for a poorly characterized ligand such as borohydride. Third, the only contribution to zfs in these LFT models is from SOC leaving out SSC,[74] which can be relatively significant, as shown below.

Quantum Chemistry Calculations: Geometry. We begin by reproducing computationally the structures of Tp*MBH_4, M = Li, Fe, Ni, and Cd at the level of ZORA/BP86 theory. Overall the optimized structures of the investigated complexes (Table 3) are in good agreement with the crystallographically determined geometries. The only exception is the lithium complex where a deviation of ∼0.1 Å for the metal−ligand distances was observed. For other complexes the average error is only 0.03 Å. The deviation of M-H and B-H distances between theory and experiment is ascribed to the large experimental errors inherent in hydrogen atom positions determined by single crystal X-ray diffraction.

For Tp*$ZnBH_4$, because there is no crystal structure available, both κ^2- and κ^3-binding modes of the BH_4^- ligand were attempted as initial structures for the geometry optimization. Significantly, both calculations converged to the same geometry, namely, a κ^2-coordinated BH_4^- ligand, reflecting that this binding mode is energetically favored in the case of the zinc complex. This finding will be supported experimentally as described below.

Quantum Chemistry Calculations: MO Description of Tp*$NiBH_4$. A molecular orbital (MO) description of Tp*$NiBH_4$ obtained from the ZORA/BP86 calculation was constructed in Figure 4, which shows that the ground state for this molecule has two singly occupied MOs (SOMOs): d_{xz}, d_{yz} (labeled 2e), consistent with its triplet spin state. Below the SOMOs in energy are fully occupied d_{xy}, $d_{x^2-y^2}$ orbitals (labeled 1e). The lowest energy MO with predominant Ni 3d character is d_{z^2} (labeled $2a_1$), giving an electronic configuration: $(d_{z^2})^2(d_{xy}, d_{x^2-y^2})^4(d_{xz}, d_{yz})^2$. This ground state configuration also results from the AOM calculation for Tp*$NiBH_4$ and is the same MO ordering as calculated for $Tp^{Ph2}FeBH_4$,[17] so that its high-spin Fe(II) electronic configuration is $(d_{z^2})^2(d_{xy}, d_{x^2-y^2})^2(d_{xz}, d_{yz})^2$. In contrast, six-coordinate, nearly octahedral $(Tp)_2Ni$ was proposed to have the following ground state electronic configuration based on gas phase photoelectron spectroscopy: $(d_{xy}, d_{x^2-y^2})^4(d_{z^2})^2(d_{xz}, d_{yz})^2$,[75] which was also proposed for four-coordinate nearly tetrahedral Tp*NiX.[65] Qualitatively, the effect of the borohydride ligand on the energy of the d_{z^2} orbital can be seen.

Inspection of the 1e MO, which is primarily Ni d_{xy}, $d_{x^2-y^2}$ in character, shows that it can be described as comprising weak π-type overlap with the pyrazole orbitals. This finding suggests that there is π-donation from the Tp^{*-} ligand; however, this effect is likely too small to be quantifiable by the AOM.

As depicted in Figure 4 and Supporting Information, Figure S5, three bridging B-H bonds functioning as π-donors strongly interact with the nickel d_{xz}- and d_{yz}-orbitals; hence, this d-orbital pair (2e) situates at the highest energy of the 3d manifold. By contrast, the axial B-H bond is involved in a σ-type interaction

dx.doi.org/10.1021/ic201775c | Inorg. Chem. 2012, 51, 2793−2805

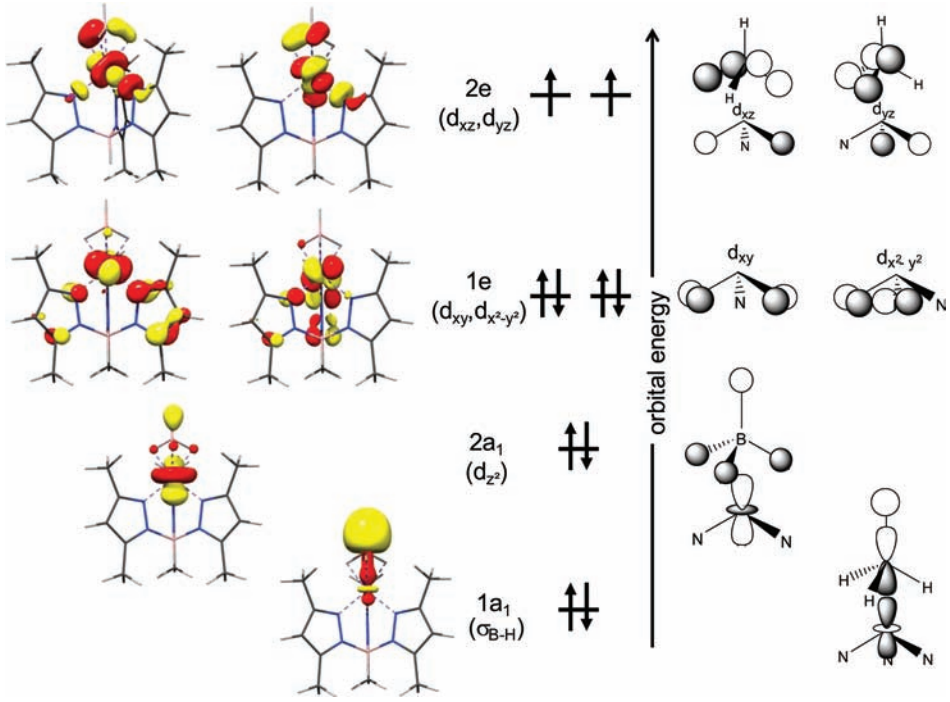

Figure 4. Frontier molecular orbitals for Tp*NiBH$_4$. The indicated orbital occupation pattern corresponds to the $^3A_2$ ground state.

with the Ni-d_{z^2} orbital. Because all donor orbitals derived from the borohydride ligand are of bonding nature, the donating electron density is largely confined within the interatomic region between the B and H atoms. As such, one may expect that the head-to-head Ni-B σ-interaction should be rather weak. In line with this, the Ni-B σ-antibonding MO ($2a_1$) is predominantly of Ni-d_{z^2} character and has the lowest energy in the Ni-3d manifold. Accordingly, its bonding partner ($1a_1$) is essentially a B-H bonding orbital.

The preceding description and a review by Xu and Lin[16] support an electronic origin for the κ^2 bonding mode of BH_4^- with $[Tp^*Zn]^+$ versus $[Tp^*Ni]^+$. Xu and Lin suggested κ^3-BH_4^- be counted as a six electron donor (in the EAN formalism) and κ^2-BH_4^- therefore be counted as a four electron donor. This formalism thus describes 18 electron $Tp^{Ph2}Fe(\kappa^3\text{-}BH_4)$ and the present 20 electron Ni(II) variant. Nickelocene (Cp_2Ni) and mixed-sandwich examples such as CpNiTp[76,77] are thermally stable, 20 electron analogues of Tp*Ni(κ^3-BH_4).

Quantum Chemistry Calculations: Zero-Field Splitting. The greatest computational challenge is to calculate the spin Hamiltonian parameters, **g**, *D*, and *E*, in Tp*NiBH$_4$. As shown in Table 1, the *g*-anisotropy is significantly underestimated by the DFT methods. For transition metal complexes, errors of a factor of ~2 in the *g*-shifts are not uncommon.[78,79] The computed *D* values using the ab initio wave function-based method reproduce both the sign and the magnitude of the experimental data for Tp*NiBH$_4$, while the DFT calculations slightly underestimate the *D* value. As noted previously,[50,80] *D* is very sensitive to minor structural changes. Comparison of the *D* values calculated using the experimental and optimized geometries revealed that the calculations at the former structure delivered slightly better results. The computed *E* values show significant deviation from experiment, but this is mainly because *E* is defined to be the difference of the two minor components of the **D** tensor, and hence the error for *E* is quite large. Since the ab initio results at the experimental geometry are in excellent agreement with experiment, the following discussion will be based only on them.

The values in Table 1 are the sum of a multitude of contributions which we unravel here. The first step is a ligand-field analysis, which is described in detail in Supporting Information. The $^3A_2$ ground state of Tp*NiBH$_4$ is characterized by half-filled Ni-d_{xz} and -d_{yz} orbitals (SOMOs; 2e in Figure 4) with additional contribution from the filled Ni-d_{xy} and -$d_{x^2-y^2}$ based orbitals (1e in Figure 4). This contribution (mixing) results from the Ni atom being 1.15 Å out of the plane defined by the three N atoms of Tp*$^-$. The most important d to d excitations involve these MOs, giving three triplet excited states: $^3A_1(1e\rightarrow2e)$, $^3A_2(1e\rightarrow2e)$, and $^3E(1e\rightarrow2e)$, and three singlet excited states: $^1A_1(1e\rightarrow2e)$, $^1A_2(1e\rightarrow2e)$, and $^1E(1e\rightarrow2e)$. Promoting one electron from $2a_1$ to 2e results in $^{1,3}E(2a_1\rightarrow2e)$. Lastly, two singlet excited states, $^1A_1(2e\rightarrow2e)$ and $^1E(2e\rightarrow2e)$, arise from spin flip transitions within 2e. The contribution of each of these excited states to the *D* value is summarized in Supporting Information, Table S2.

From among these excitations, there are two dominant SOC contributions: $^3A_1(1e\rightarrow2e)$ and $^3E(1e\rightarrow2e)$, each with a magnitude >50 cm^{-1} (by CASSCF, see Supporting Information, Table S2), but with opposite sign, respectively positive and negative, so that they nearly cancel out. The next largest-magnitude contributions (ca. 14 cm^{-1} by CASSCF) are from the two singlet transitions, $^1A_1(2e\rightarrow2e)$ and $^1E(2e\rightarrow2e)$, but these again are of opposite sign and thus nearly cancel. The significant magnitude contribution from spin-flip transitions (albeit opposite in sign) is counter to the common assumption that zfs is dominated by excited states of the same spin as the ground state, at least for non-Kramers systems. The remaining SOC contributions are very small in magnitude ($\leq$0.2 cm^{-1}), so that the total calculated D^{SOC} value is small (Supporting Information, Table S2).

As a result of this near cancellation of the SOC contributions, the computed SSC component (0.3 cm^{-1}; see Table 1) accounts for ~20% of the total *D* value, and therefore cannot be neglected for any quantitative treatment. This corroborates what is found for other transition metal systems with overall small magnitude *D*.[74,80,81]

dx.doi.org/10.1021/ic201775c | Inorg. Chem. 2012, 51, 2793−2805

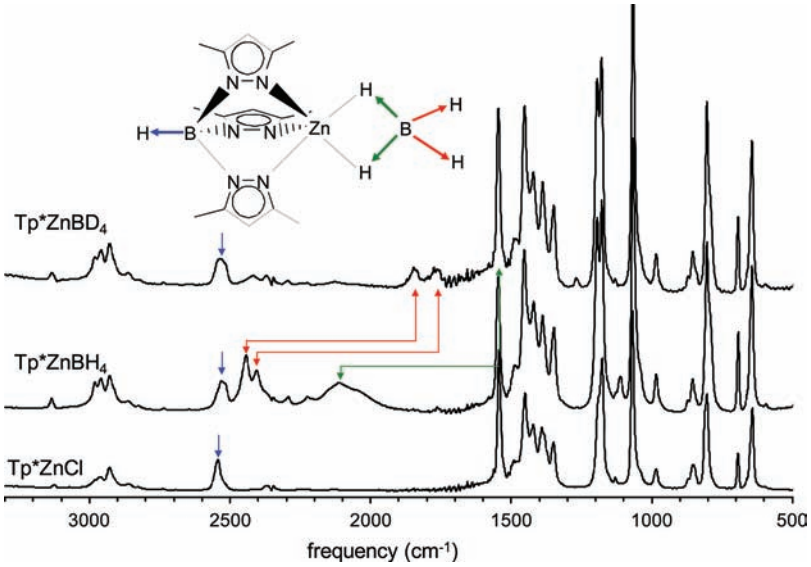

Figure 5. Infrared spectra of Tp*ZnCl (bottom), Tp*Zn(κ^2-BH_4) (middle), and Tp*Zn(κ^2-BD_4) (top) as KBr pellets. The signature ν(B-H) band from the Tp* ligand is marked by a blue arrow; red and green arrows mark the ν(B-H_t) and ν(B-H_b) bands, respectively. These arrows also indicate the ν(B-$H_{t,b}$) to ν(B-$D_{t,b}$) shift.

Synthesis of Tp*Zn(κ^2-BH_4). The preparation and characterization of Tp*ZnBH_4 experimentally validates the DFT results (vide supra). The two phase approach (solid $NaBH_4$ + Tp*ZnCl/CH_2Cl_2 solution) was necessary to make Tp*ZnBH_4. An alternative route in which equimolar amounts of Tp*ZnCl and [NBu_4]BH_4 were dissolved in dichloromethane failed to yield any product over the course of 24 h at room temperature. Rupture of the Zn-Cl bond may be rate limiting and facilitated in the two-phase mixture by Tp*Zn-Cl(δ^-)···$^+$Na ion-dipole forces. The two-phase method likely benefits from both the polarizing sodium ions[82] and the enthalpic driving force of the NaCl lattice that forms when borohydride is extracted from the solid.

Vibrational Spectroscopy of Tp*M(BH_4, BD_4): Experiment and Theory. Infrared measurements in the solid state confirmed the κ^2-BH_4^- coordination mode for Tp*ZnBH_4 (Figure 5). The pattern and frequencies of ν(B-H) vibrations in the 2500−2000 cm^{-1} region match those seen for the structurally characterized Tp*Cd(κ^2-BH_4)[18] and fit the general patterns described in the review by Marks and Kolb.[1] The pair of bands near 2400 cm^{-1} is thus assigned to the asymmetric and symmetric ν(B-H_t) (t = terminal) vibrations of κ^2-BH_4^-. A broad band near 2100 cm^{-1} is assigned to ν(B-H_b) (b = bridging) in Tp*Zn(κ^2-BH_4).

Band shifts seen in the deuterated complex, Tp*Zn(κ^2-BD_4) (Figure 5) confirmed that these vibrations result from the coordinated borohydride ion. Deuterium substitution shifted the ν(B-H_t) pair from 2442 and 2405 cm^{-1} to ν(B-D_t) at 1841 and 1766 cm^{-1} (within 2% of the values predicted by Hooke's Law: 1802 and 1775 cm^{-1}; $\nu_{B\text{-}D}/\nu_{B\text{-}H}$ = 0.74).[83] The broad ν(B-D_b) feature of Tp*Zn(κ^2-BD_4) therefore shifts to a spectral region obscured by the rich ligand fingerprint bands.

The computed symmetric and antisymmetric stretching frequencies for the terminal hydrogen atoms are ν_{Cal}(B-H_t) = 2449 and 2514 cm^{-1}, respectively, and those for the bridging are ν_{Cal}(B-H_b) = 2118 and 2212 cm^{-1}, respectively. The experimentally observed isotope shifts of these vibrations were also successfully reproduced by the calculations: ν_{Cal}(B-D_t) = 1883, 1787 cm^{-1} vs ν_{Exp}(B-D_t) = 1841, 1766 cm^{-1}; ν_{Cal}(B-D_b) = 1631, 1535 cm^{-1}, which would overlap with Tp*$^-$ vibrational bands and explain the inability to resolve this feature experimentally. Thus, the calculations not only confirm the assignment of the vibrations but also lend further credence for the proposed κ^2 binding mode of the borohydride ligand in Tp*ZnBH_4.

The solid state IR spectra of Tp*Ni(κ^3-BH_4) and Tp*Ni(κ^3-BD_4) have been reported earlier,[15] but not discussed in the context of variable borohydride denticity. Figure 6 presents the solid state IR spectra of Tp*Ni(κ^3-BH_4) and Tp*Ni(κ^3-BD_4). The feature at 2400 cm^{-1} assigned to ν(B-H_t) for the zinc protio complex is completely *absent* in the spectrum of the nickel congener, confirming that the zinc complex binds borohydride in a manner distinct from the structurally characterized nickel(II) complex. The band assigned to ν(B-H_b) in the zinc complex is found in the spectrum of the nickel complex, albeit shifted to lower frequency because of the greater electron sharing by hydrogen atoms in the tridentate coordination mode. The band assigned to ν(B-H_t) at 2500 cm^{-1} shifts to 1900 cm^{-1} for ν(B-D_t), as expected. In all spectra, the ν(B-H) band of the Tp*$^-$ ligand is a nearly invariant internal standard.

IR spectra recorded in dichloromethane solution show that the behavior of the two metal complexes in solution is the same as in the solid state, corroborating electronic spectra of the Ni complex (Supporting Information, Figure S1). This can be seen in Supporting Information, Figures S6 and S7, which present the solution-phase IR spectra for Tp*Zn(κ^2-BH_4, BD_4) and Tp*Ni-(κ^3-BH_4, BD_4), respectively. In particular, solution IR spectra of Tp*ZnBH_4 (Supporting Information, Figure S6) show exactly the same κ^2 ν(B-H) vibrational pattern and at essentially the same frequencies (2441, 2403, 2125 cm^{-1}) as in the solid state.

NMR Characterization and Borohydride Exchange Processes. NMR measurements further confirmed the formation of Tp*ZnBH_4 and helped to characterize solution-phase behavior of both zinc and nickel borohydrides. Consistent with the IR results, room temperature NMR results for Tp*ZnBH_4 (Figure 7, top spectrum) are nearly identical to those reported for structurally characterized Tp*CdBH_4.[18]

dx.doi.org/10.1021/ic201775c | *Inorg. Chem.* 2012, 51, 2793−2805

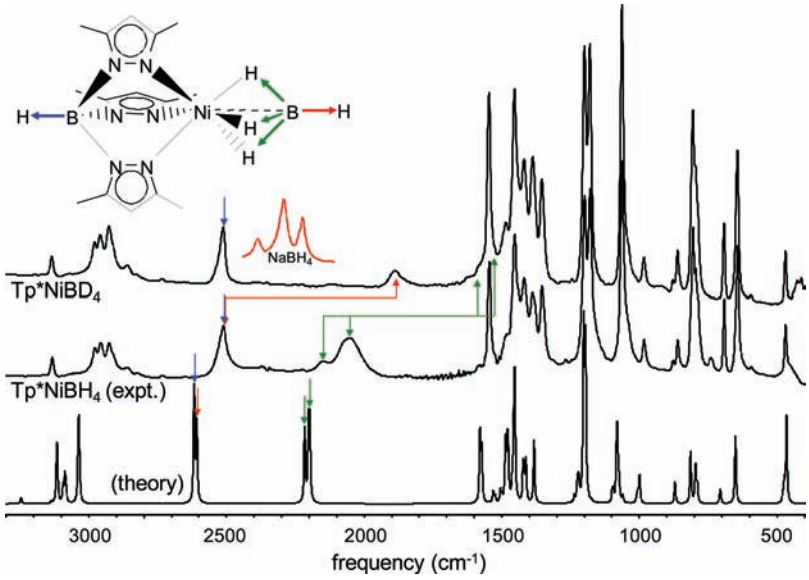

Figure 6. Infrared spectra of Tp^*NiBD_4 (top) and Tp^*NiBH_4 (middle) as KBr pellets. The bottom spectrum is calculated based on the optimized geometry for Tp^*NiBH_4. The ν(B-H) stretching modes are indicated in the molecular sketch and labeled correspondingly with colored arrows. Inset in red is the ν(B-H) spectral region observed for $NaBH_4$ (KBr pellet). The $\nu(B\text{-}H_t)$ bands for Tp* and BH_4 are unresolved in this matrix, but are resolved for spectra taken of samples in CH_2Cl_2 solution (Supporting Information, Figure S7).

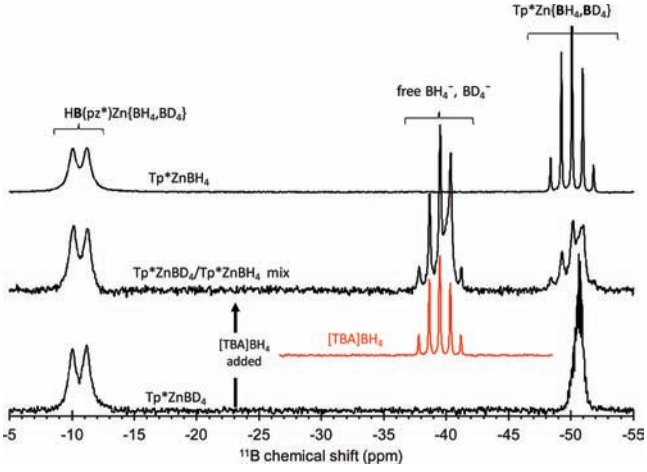

Figure 7. ^{11}B NMR spectra in CD_2Cl_2 solution of Tp^*ZnBH_4 (top) and Tp^*ZnBD_4 (bottom) and after the addition of 1 equiv of tetra-*n*-butylammonium borohydride (middle). Peak assignments are indicated, and the spectrum of $[NBu_4]BH_4$ in CD_2Cl_2 is shown as a red inset. Both free borohydride from $[NBu_4]BH_4$ and the zinc-coordinated borohydride resonances show the effects of BH_4^-/BD_4^- interconversion.

All measurements confirm persistent but fluxional zinc-borohydride coordination in solution on the NMR time scale. The ^{11}B signal for coordinated borohydride is shifted significantly upfield relative to the free BH_4^- quintet observed for $[NBu_4]BH_4$ (δ = −39.5 ppm, $J_{B\text{-}H}$ = 81 Hz) in the same solvent. Similarly ^1H and ^{13}C NMR spectra (Supporting Information, Figures S8 and S9, respectively) both show a highly symmetric (C_{3v}) Tp^*ZnBH_4 coordination sphere. The 1:1:1:1 quartet assigned to coordinated borohydride in the proton spectrum (δ = 0.68 ppm, $J_{H\text{-}B}$ = 83 Hz) confirms the equivalence of all hydrogen atoms because of rapid interconversion of H_t and H_b coordinated to the metal. These hydrogen atoms are deshielded relative to free borohydride of $[NBu_4]BH_4$ (δ = −0.20 ppm, quartet), consistent with increased electron density on boron when coordinated in Tp^*ZnBH_4 versus the ionic system. Collectively these results suggest that no dissociated ion pair, $[Tp^*Zn]^+$ BH_4^-, exists to any great extent in this mixture. The strong Lewis acidity of a coordinatively unsaturated $[Tp^*Zn]^+$ species almost certainly precludes this.

Solution-phase infrared and variable temperature ^{11}B NMR measurements respectively provide maximum and minimum lifetimes (τ) of a single $Tp^*Zn(\kappa^2\text{-}BH_4)$ conformer in solution. The correspondence between room temperature solid state and solution IR spectra of Tp^*ZnBH_4 (Figure 5 and Supporting Information, Figure S6, respectively) places the lower limit of the lifetime of a single κ^2 conformer at $\tau \geq 10^{-13}$ s. At the upper limit, the ^{11}B NMR quintet of coordinated borohydride persisted on cooling the dichloromethane solution even to −85 °C (with some line broadening). In addition, the doublet of the ligand Tp*-boron ($J_{B\text{-}H}$ = 110 Hz, typical pseudo tetrahedral Tp*ZnX) resonance coalesces into a single broad resonance at −50 °C with no change in chemical shift. These results collectively place the lifetime of a single conformer on the order of $10^{-8} \geq \tau \geq 10^{-13}$ s.

The association of borohydride with zinc in Tp^*ZnBH_4 was further tested by an exchange experiment involving the reaction of Tp^*ZnBD_4 with $[NBu_4]BH_4$ in CD_2Cl_2 (Figure 7). Prior to the addition of the borohydride salt, ^2H and ^{11}B NMR spectra of Tp^*ZnBD_4 gave resonances comparable to Tp^*ZnBH_4 in the same solvent. Specifically, ^2H NMR (Supporting Information, Figure S10) showed a bound borodeuteride at δ = 0.70 ppm (quartet, $J_{B\text{-}D}$ = 12 Hz). The addition of 1 equiv of $[NBu_4]BH_4$ to this mixture resulted in a rapid change (within 10 min). The original ^2H signal from bound BD_4^- was replaced by a broad featureless resonance centered at about 0.3 ppm. This resonance is intermediate between the values of bound and unbound ion (δ = −0.20 ppm, assuming $\delta_D \sim \delta_H$ for this ion) in this same solvent. The ^{11}B NMR spectrum of this mixture shows the original multiplet of bound BD_4^- (Figure 7, bottom spectrum; an expansion of this region is shown in Supporting Information, Figure S11) to be replaced by a complex multiplet at the same

dx.doi.org/10.1021/ic201775c | Inorg. Chem. 2012, 51, 2793−2805

chemical shift (Figure 7, middle spectrum). Although this multiplet could not be fully resolved, it appears to be a superposition of the quintet seen in Tp*ZnBH$_4$ and the narrower resonance originally seen for Tp*ZnBD$_4$. This observation is consistent with the formation of a mixture of Tp*ZnBH$_4$ and Tp*ZnBD$_4$ (where $J_{B\text{-}H}$ = 83 Hz vs $J_{B\text{-}D}$ about 15% of that value in the original borodeuteride). A new resonance near −40 ppm also appears. It too is a complex multiplet, incompletely resolved into the sharp quintet or approximate nonet of free BH_4^- or BD_4^-, respectively. These data can be summarized in the following reaction, whose equilibrium constant must be near unity and for which there must be only a small barrier to interconversion.[84]

$$Tp^*ZnBD_4 + BH_4^- \leftrightarrows Tp^*ZnBH_4 + BD_4^-$$

Similar exchange behavior was observed in the case of Tp*NiBH$_4$, albeit with the added complexity of significant paramagnetic shifts in the coordinated borohydride ^{11}B NMR resonance (Figure 8). As for the zinc(II) system, distinct

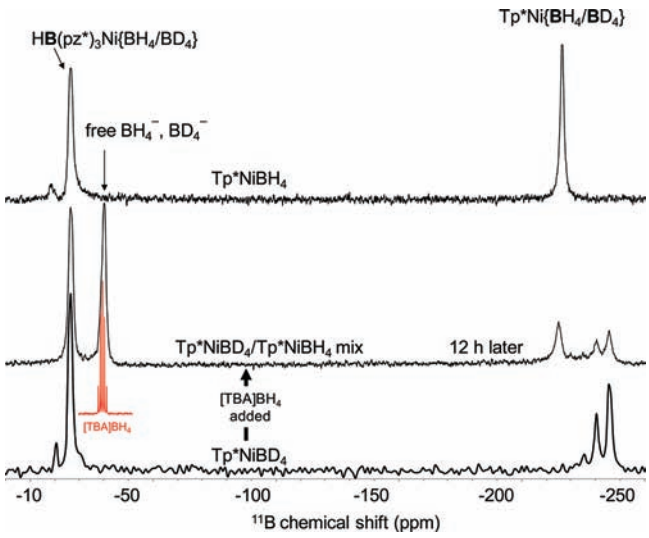

Figure 8. Paramagnetic ^{11}B NMR in CD_2Cl_2 solution of Tp*NiBH$_4$ (top) and Tp*NiBD$_4$ (bottom). Peak assignments are indicated. The middle spectrum demonstrates the effect after 12 h of adding 1 equiv of [NBu$_4$]BH$_4$ to Tp*NiBD$_4$. The spectrum of [NBu$_4$]BH$_4$ in CD_2Cl_2 is shown as a red inset. The resonance assigned to free borohydride at −39.5 ppm is a complex multiplet and not the clean quintet seen for pure BH_4^-, representing a mixture of BH_4^- and BD_4^-.

resonances are observed for the Tp*-boron and for the borohydride/borodeuteride boron atoms of Tp*Ni(BH$_4$, BD$_4$) in dichloromethane solution. The Tp*-boron resonance is centered near −26 ppm whereas the coordinated BH_4^-/BD_4^- signal is shifted upfield to −240 ± 10 ppm (Figure 8). The addition of 1 equiv of [NBu$_4$]BH$_4$ to a solution of Tp*NiBD$_4$ resulted in the appearance of a free BH_4^-/BD_4^- multiplet resonance near −40 ppm and a change in the nickel-bound BH_4^-/BD_4^- resonance to a pair of resonances suggesting a resultant mixture of Tp*NiBH$_4$ and Tp*NiBD$_4$ (Figure 8). We have recently observed that in Tp*NiX, the ^{11}B resonances from Tp*$^-$ are extremely sensitive to both coordination geometry and the identity of X.[85] Therefore, the invariant chemical Tp*-boron resonance for Tp*Ni(BH$_4$, BD$_4$) strongly suggests a primary chemical environment for Tp* throughout the exchange process. These NMR data make clear that the intact borohydride ion is persistently associated with the metal ion for Tp*MBH$_4$, without exchange of individual H atoms (H^- ions), and that the barrier to exchange of metal-bound with free borohydride is low in solution at room temperature.

As a final comment, we note that the ^{11}B chemical shift of the Ni-coordinated borohydride/borodeuteride is sensitive to isotopologue, with a difference of about 20 ppm between the two (Figure 8). This solution phase NMR measurement suggests a difference in electronic structure between the two isotopologues that is qualitatively in agreement with the difference between the two seen in the solid state by HFEPR. It may be that the differences between Ni(II) coordination by BH_4^- vs BD_4^- are more fundamental than merely crystal packing effects.

Bonding Descriptions of Tp*MBH$_4$ and Reactivity Implications. The present nickel and zinc results and the reported iron and cadmium complexes demonstrate that the Tp^{R}MBH$_4$ coordination sphere is well suited for the preparation of stable metal borohydrides. To date κ^2 and κ^3 BH_4^- coordination modes only have been observed in these systems.[86] As predicted by both Marks and Kolb[1] and Xu and Lin,[16] κ^3 BH_4^- coordination leads to shorter metal-boron distances than κ^2. Both of these reviews outlined the type of metal d and borohydride orbital overlap expected in such cases. Experimental metal-boron distances are within range for covalent interactions, compared to metal-nitrogen distances in the same molecule and allowing for the larger covalent radius of boron vs nitrogen. While short distances alone do not prove metal-boron bonds.[87,88] MO descriptions of the iron and the nickel cases predict reasonable covalent metal-boron interactions. The credibility of these models is further substantiated by their accurate prediction of an array of experimental spectroscopic characteristics for nickel. Hydrogen release by thermolysis of lithium borohydride was enhanced by the presence of iron(II) and nickel(II) ion dopants, and formation of metal-borides was a thermodynamic advantage in this process.[89] The close metal-boron contacts in Tp^{R}MBH$_4$ could be models of such nascent metal-borides.

The scorpionate coligand clearly influences the metal-borohydride interaction in these systems. Frontier MOs in both the iron and nickel cases show a d-orbital manifold modulated by Tp^{R-}. This may be seen in Figure 4 where the degenerate SOMOs involve Ni-Tp* σ (N lone pair) and Ni-BH$_4$ π interactions. Metal-BH$_4$ σ interaction is limited to d-orbitals with a component along the 3-fold (z) axis of the molecule. Noticeably absent in the zinc κ^2 case is any d_{z^2} overlap with BH_4^- (Supporting Information, Figure S12). Therefore, it appears that the formation and stability of Tp^{R}M(κ^3-BH$_4$) is driven by higher energy partially occupied d_{xz}, d_{yz}, and d_{z^2} orbitals receptive to the π and σ electron donation from the BH_4^- nucleophile. The role of the Tp^{R-} ligand is seen as raising the energies of the d_{xz} and d_{yz} orbitals sufficiently to prevent outright metal ion reduction by borohydride. The standard reduction potential for the Ni(II/0) couple is −0.26 V and for the Fe(II/0) couple is −0.44 V, which suggests that reduction by borohydride is possible for both metal(II) ions (we have observed it for Ni(II)). Isolation of stable Tp^{R}M^{II}BH$_4$ (M = Fe and Ni) thus emphasizes the important reduction-modulating role of the coordinated Tp-ligand.[90]

Solution phase experiments are consistent with the weak ligand field imposed by coordinated borohydride versus Tp*$^-$. Despite rapid interconversion of conformers and the rapid exchange of BH_4^- for BD_4^- in a particular Tp*M(κ^n-BH$_4$) system, the ligand ^{11}B NMR resonance is invariant and its infrared ν(B-H) band is similarly unchanged. Steric effects from the scorpionate can play only a minimal, if any, role in this

dx.doi.org/10.1021/ic201775c | Inorg. Chem. 2012, 51, 2793−2805

interconversion and exchange. This is most likely due to the small barrier to interconversion, making the predictably more reactive bridging H atoms nearly as accessible in solution as the terminal H atom(s).

The nickel case shows additional characteristics supporting electron donation by borohydride. Previous reports described the tendency of Tp^*NiBH_4 to reduce simple halocarbons (CCl_4 and $CHCl_3$, but not CH_2Cl_2) by a radical mechanism resulting in Tp*NiCl formation.[15] Analogous reactivity is shown by Tp^RCu^I complexes, which catalyze radical addition to olefins.[91] A key step in this process was the cycling of the copper(I) center through a readily accessible copper(II) oxidation state, involving the abstraction of a halogen atom leading to a transient $[Tp^RCu^{II}X]$ species. While (II/I) redox behavior is more common for copper scorpionates, the parallel reactivity behavior of these two metal systems invites the comparison to the present nickel case.

We have observed $LiAlH_4$ to reductively decompose Tp*NiCl into nickel metal and Raney nickel-like solids, suggesting that the stability of Tp^*NiBH_4 is a balance between reduction of nickel(II) and simple borohydride coordination controlled by the Tp^{*-} ligand. Aluminohydride is too strong an electron donor in the nickel case. No reduction is expected in the zinc case, and isolation of Tp^*ZnAlH_4 would be an intriguing test of this hypothesis.

CONCLUSIONS

In this work, a detailed combination of experimental, quantum chemical, and ligand-field theory analysis of a paramagnetic nickel(II) scorpionate complex with a κ^3-BH_4^- ligand, Tp^*NiBH_4, has been performed. Analysis of the frontier orbitals of the complex revealed that the coordinated borohydride employs its four B-H bonding orbitals to donate electron density to the metal center leading to both π- and σ-type bonding. Although the latter interaction is rather weak, the coordinated κ^3-BH_4^- ligand is best rationalized as a tetradentate ligand.

Magnetic resonance measurements and quantum chemical calculations described the relative contributions of spin and orbital angular momenta to the magnetic properties of Tp^*NiBH_4. HFEPR spectroscopy allowed accurate determination of the zfs in the $S = 1$ nickel(II) complex, which was found to be relatively small in magnitude and positive: $D = +1.91\ cm^{-1}$, $|E/D| = 0.15$. Quantum chemical calculations allowed for deconvolution of the multiple contributing factors to the zfs in this system. These calculations demonstrated that the low D value observed is the resultant sum of several large but opposite sign SOC contributions, so that the SSC contribution is non-negligible and indeed accounts for approximately one-fifth of the final D value.

A zinc(II) analogue, Tp^*ZnBH_4, is also reported. The bonding mode of BH_4^- in this complex is distinctly different from that in the nickel congener, conclusively demonstrated by solid and solution phase and computational infrared analyses. Previous reports have suggested that the κ^2-borohydride and κ^3-borohydride anion can be counted as four electron and six electron donors, respectively, in the effective atomic number counting scheme.[16] Such an EAN description is supported by the present models of Tp^*NiBH_4 (formally 20 electron species). This description predicts reduced electron donation from borohydride to the $3d^{10}$ zinc(II) ion, and $Tp^*Zn(\kappa^2\text{-}BH_4)$ results. The present theoretical and spectroscopic descriptions demonstrate that the Tp^RMBH_4 system is suited for the preparation of a variety of other stable metal borohydrides.

ASSOCIATED CONTENT

Supporting Information

Ligand-field analysis of Tp^*NiBH_4, metrical parameters for Tp^*NiBH_4 used in AOM analysis; contributions to D in Tp^*NiBH_4; figures showing visible−NIR spectra of Tp^*NiBH_4 (solution and solid state); MO diagrams of BH_4^-; comparison HFEPR spectra of $Tp^*Ni(BH_4,BD_4)$; HFEPR spectrum of Tp^*NiBD_4; resonant field versus frequency dependence of Tp^*NiBD_4; solution IR spectra of $Tp^*(Ni,Zn)(BH_4,BD_4)$; ^1H, ^{13}C, ^2H, and ^{11}B NMR spectra of $Tp^*Zn(BH_4,BD_4)$; calculated MO diagram for Tp^*ZnBH_4. This material is available free of charge via the Internet at http://pubs.acs.org.

AUTHOR INFORMATION

Corresponding Authors

*E-mail: patrickd@uca.edu (P.J.D.), jtelser@roosevelt.edu (J.T.).

Notes

The authors declare no competing financial interest.

ACKNOWLEDGMENTS

This work has been supported by National Science Foundation under CHE-0717213 (P.J.D.) and by the donors of the Petroleum Research Fund, administered by the American Chemical Society (Grant 35602-B3, P.J.D.). The NMR used for all measurements was also funded by the NSF (Grant CCLI 0125711). HFEPR measurements at the NHMFL were funded by the NSF (Cooperative Agreement DMR 0654118), the State of Florida, and DOE. J.K. and J.T. received additional funds from User Collaboration Grant 5062. The 25-T resistive magnet was funded by the W. Keck Foundation. The UV−vis−NIR spectrophotometer at Roosevelt University was obtained thanks to the Goldenberg Foundation. S.Y. and F.N. acknowledge the financial support from the collaborative research center SFB 813 ("Chemistry at spin centers").

REFERENCES

(1) Marks, T. J.; Kolb, J. R. *Chem. Rev.* **1977**, *77*, 263−293.
(2) Ganem, B.; Osby, J. O. *Chem. Rev.* **1986**, *86*, 763−780.
(3) Grochala, W.; Edwards, P. P. *Chem. Rev.* **2004**, *104*, 1283−1316.
(4) Orimo, S.-i.; Nakamori, Y.; Eliseo, J. R.; Züttel, A.; Jensen, C. M. *Chem. Rev.* **2007**, *107*, 4111−4132.
(5) Staubitz, A.; Robertson, A. P. M; Manners, I. *Chem. Rev.* **2010**, *110*, 4079−4124.
(6) Keaton, R. J.; Blacquiere, J. M.; Baker, R. T. *J. Am. Chem. Soc.* **2007**, *129*, 1844−1845.
(7) Petró, J. The Raney-Nickel. In *Catalysis of Organic Reactions*; Ford, M. E., Ed.; Marcel Dekker Inc.: New York, 2001; Vol. *82*, pp 1−34.
(8) Here the kappa (κ) notation is employed specifically to refer to the number of hydrogen atoms from borohydride that are coordinated to the metal center. This does not preclude the possibility of delocalized bonding participation from boron. We also note that other workers use the eta (η) notation, rather than kappa.
(9) Curtis, N. F. *J. Chem. Soc.* **1965**, 924−931.
(10) The borohydride complexes reported by Curtis were of Ni(II) with cyclic tetraamine or noncyclic tetradentate Schiff base amine ligands; representative complexes are: 5,7,7,12,14,14-hexamethyl-1,4,8,11-tetra-azacyclotetradecanenickel(II) borohydride perchlorate and 4,6,6-trimethy1-3,7-diazanon-3-ene-1,9-diaminenickel(II) borohydride perchlorate.
(11) Journaux, Y.; Lozan, V.; Klingele, J.; Kersting, B. *Chem. Commun.* **2006**, 83−84.

(12) Kandiah, M.; McGrady, G. S.; Decken, A.; Sirsch, P. *Inorg. Chem.* **2005**, *44*, 8650−8652.
(13) Holah, D. G.; Hughes, A. N.; Hui, B. C.; Wright, K. *Can. J. Chem.* **1974**, *52*, 2990−2999.
(14) Ligand abbreviations used: Tp^- = hydrotrispyrazolylborate; Tp^{*-} = hydrotris(3,5-dimethylpyrazolyl)borate; Tp^{PhMe-} = hydrotris(3-phenyl-5-methylpyrazolyl)borate; Tp^{Ph2-} = hydrotris(3,5-diphenylpyrazolyl)borate; Tpm = tris(pyrazolyl)methane; Tpm* = tris(*N*-3,5-dimethylpyrazolyl)methane; $PhB(CH_2PPh_2)_3^-$ = phenyltris(diphenylphosphinomethyl)borate.
(15) Desrochers, P. J.; LeLievre, S.; Johnson, R. J.; Lamb, B. T.; Phelps, A. L.; Cordes, A. W.; Gu, W.; Cramer, S. P. *Inorg. Chem.* **2003**, *42*, 7945−7950.
(16) Xu, Z.; Lin, Z. *Coord. Chem. Rev.* **1996**, *156*, 139−162.
(17) Mehn, M. P.; Brown, S. D.; Paine, T. K.; Brennessel, W. W.; Cramer, C. J.; Peters, J. C.; Que, L. Jr. *Dalton Trans.* **2006**, 1347−1351.
(18) Reger, D. L.; Mason, S. S.; Rheingold, A. L. *J. Am. Chem. Soc.* **1993**, *115*, 10406−10407.
(19) Trofimenko, S. *J. Am. Chem. Soc.* **1967**, *89*, 6288−6294.
(20) Brand, U.; Rombach, M.; Seebacher, J.; Vahrenkamp, H. *Inorg. Chem.* **2001**, *40*, 6151−6157.
(21) Brand, U.; Rombach, M.; Vahrenkamp, H. *Chem. Commun.* **1998**, 2717−2718.
(22) Sutton, C. A.; Desrochers, P. J., unpublished results. In the case of nickel, whose complexes are brightly colored, bright pink Tp*NiCl solutions yield bright green solutions containing Tp^*NiBH_4 (confirmed by UV-vis) after less than 2 min of vigorous stirring.
(23) Zvyagin, S. A.; Krzystek, J.; van Loosdrecht, P. H. M.; Dhalenne, G.; Revcolevschi, A. *Physica B* **2004**, *346*−*347*, 1−5.
(24) Hassan, A. K.; Pardi, L. A.; Krzystek, J.; Sienkiewicz, A.; Goy, P.; Rohrer, M.; Brunel, L.-C. *J. Magn. Reson.* **2000**, *142*, 300−312.
(25) Abragam, A.; Bleaney, B. *Electron Paramagnetic Resonance of Transition Ions*; Dover Publications, Inc.: Mineola, NY, 1986.
(26) Krzystek, J.; Zvyagin, S. A.; Ozarowski, A.; Trofimenko, S.; Telser, J. *J. Magn. Reson.* **2006**, *178*, 174−183.
(27) Bendix, J.; Brorson, M.; Schäffer, C. E. *Inorg. Chem.* **1993**, *32*, 2838−2849.
(28) Figgis, B. N.; Hitchman, M. A. *Ligand Field Theory and its Applications*; Wiley-VCH: New York, 2000.
(29) Mabbs, F. E.; Collison, D. *Electron Paramagnetic Resonance of d Transition Metal Compounds*; Elsevier: Amsterdam, The Netherlands, 1992. This text provides the following values for Racah parameters for Ni^{2+}: B = 1080 cm^{-1}, $C = 4.5B$, which differ modestly from those used here.
(30) Brorson, M.; Schäffer, C. E. *Inorg. Chem.* **1988**, *27*, 2522−2530.
(31) Neese, F. *ORCA - an ab initio, Density Functional and Semiempirical Program Package*, 2.8.0; Universität Bonn: Bonn, Germany, 2010.
(32) Becke, D. A. *Phys. Rev. A* **1988**, *38*, 3098−3100.
(33) Perdew, J. P. *Phys. Rev. B* **1986**, *33*, 8822−8824.
(34) Perdew, J. P. *Phys. Rev. B* **1986**, *34*, 7406.
(35) van Lenthe, E.; Baerends, E. J.; Snijders, J. G. *J. Chem. Phys.* **1993**, *99*, 4597−4610.
(36) van Lenthe, E.; Baerends, E. J.; Snijders, J. G. *J. Chem. Phys.* **1994**, 101.
(37) van Lenthe, E.; van Leeuwen, R.; Baerends, E. J.; Snijders, J. G. *Int. J. Quantum Chem.* **1996**, *57*, 281−293.
(38) Pantazis, D. A.; Neese, F. *J. Chem. Theory Comput.* **2009**, *5*, 229−238.
(39) Pantazis, D. A.; Chen, X. Y.; Landis, C. R.; Neese, F. *J. Chem. Theory Comput.* **2008**, *4*, 908−919.
(40) Eichkorn, K.; Treutler, O.; Öhm, H.; Häser, M.; Ahlrichs, R. *Chem. Phys. Lett.* **1995**, *242*, 652−660.
(41) Eichkorn, K.; Weigend, F.; Treutler, O.; Ahlrichs, R. *Theor. Chem. Acc.* **1997**, *97*, 119−124.
(42) Eichkorn, K.; Treutler, O.; Öhm, H.; Häser, M.; Ahlrichs, R. *Chem. Phys. Lett.* **1995**, *240*, 283−289.
(43) McWeeny, R.; Mizuno, Y. *Proc. R. Soc. Lond. A* **1961**, *259*, 554−577.
(44) Sinnecker, S.; Neese, F. *J. Phys. Chem. A* **2006**, *110*, 12267−12275.
(45) Neese, F. *J. Chem. Phys.* **2007**, *127*, 164112.
(46) Hess, B. A.; Marian, C. M.; Wahlgren, U.; Gropen, O. *Chem. Phys. Lett.* **1996**, *251*, 365−371.
(47) Berning, A.; Schweizer, M.; Werner, H.-J.; Knowles, P. J.; Palmieri, P. *Mol. Phys.* **2000**, *98*, 1823−1833.
(48) Neese, F. *J. Chem. Phys.* **2005**, *122*, 034107.
(49) Ganyushin, D.; Neese, F. *J. Chem. Phys.* **2006**, *125*, 024103.
(50) Ye, S.; Neese, F.; Ozarowski, A.; Smirnov, D.; Krzystek, J.; Telser, J.; Liao, J.-H.; Hung, C.-H.; Chu, W.-C.; Tsai, Y.-F.; Wang, R.-C.; Chen, K.-Y.; Hsu, H.-F. *Inorg. Chem.* **2010**, *49*, 977−988.
(51) Angeli, C.; Cimiraglia, R.; Evangelisti, S.; Leininger, T.; Malrieu, J.-P. *J. Chem. Phys.* **2001**, *114*, 10252−10264.
(52) Angeli, C.; Cimiraglia, R.; Malrieu, J.-P. *J. Chem. Phys.* **2002**, *117*, 9138−9153.
(53) Ganyushin, D.; Gilka, N.; Taylor, P. R.; Marian, C. M.; Neese, F. *J. Chem. Phys.* **2010**, *132*, 144111.
(54) Kottis, P.; Lefebvre, R. *J. Chem. Phys.* **1964**, *41*, 379−393.
(55) Krzystek, J.; Park, J.-H.; Meisel, M. W.; Hitchman, M. A.; Stratemeier, H.; Brunel, L.-C.; Telser, J. *Inorg. Chem.* **2002**, *41*, 4478−4487.
(56) van Dam, P. J.; Klaassen, A. A. K.; Reijerse, E. J.; Hagen, W. R. *J. Magn. Reson.* **1998**, *130*, 140−144.
(57) Limburg, J.; Vrettos, J. S.; Crabtree, R. H.; Brudvig, G. W.; de Paula, J. C.; Hassan, A.; Barra, A.-L.; Duboc-Toia, C.; Collomb, M.-N. *Inorg. Chem.* **2001**, *40*, 1698−1703.
(58) Krzystek, J.; Ozarowski, A.; Telser, J. *Coord. Chem. Rev.* **2006**, *250*, 2308−2324.
(59) Tregenna-Piggott, P. L. W.; Weihe, H.; Bendix, J.; Barra, A.-L.; Güdel, H.-U. *Inorg. Chem.* **1999**, *38*, 5928−5929.
(60) Tregenna-Piggott, P. L. W.; Spichiger, D.; Carver, G.; Frey, B.; Meier, R.; Weihe, H.; Cowan, J. A.; McIntyre, G. J.; Zahn, G.; Barra, A.-L. *Inorg. Chem.* **2004**, *43*, 8049−8060.
(61) The difference between isotopologues may not be only a solid state effect.
(62) Lever, A. B. P. *Inorganic Electronic Spectroscopy*, 2 ed.; Elsevier: Amsterdam, The Netherlands, 1984; pp. 336, 339.
(63) Lever, A. B. P.; Walker, I. M.; McCarthy, P. J.; Mertes, K. B.; Jircitano, A.; Sheldon, R. *Inorg. Chem.* **1983**, *22*, 2252−2258.
(64) Martin, L. Y.; Sperati, C. R.; Busch, D. H. *J. Am. Chem. Soc.* **1977**, *99*, 2968−2981.
(65) Desrochers, P. J.; Telser, J.; Zvyagin, S. A.; Ozarowski, A.; Krzystek, J.; Vicic, D. A. *Inorg. Chem.* **2006**, *45*, 8930−8941.
(66) Ballhausen, C. J. In *Introduction to Ligand Field Theory*; McGraw-Hill: New York, 1962; pp 99−103.
(67) Schäffer, C. E. *Struct. Bonding (Berlin)* **1968**, *5*, 68−95.
(68) Nieto, I.; Bontchev, R. P.; Ozarowski, A.; Smirnov, D.; Krzystek, J.; Telser, J.; Smith, J. M. *Inorg. Chim. Acta* **2009**, *362*, 4449−4460.
(69) Larrabee, J. A.; Alessi, C. M.; Asiedu, E. T.; Cook, J. O.; Hoerning, K. R.; Klingler, L. J.; Okin, G. S.; Santee, S. G.; Volkert, T. L. *J. Am. Chem. Soc.* **1997**, *119*, 4182−4196.
(70) Krzystek, J.; Swenson, D. C.; Zvyagin, S. A.; Smirnov, D.; Ozarowski, A.; Telser, J. *J. Am. Chem. Soc.* **2010**, *132*, 5241−5253.
(71) Fujihara, T.; Schönherr, T.; Kaizaki, S. *Inorg. Chim. Acta* **1996**, *249*, 135−141.
(72) Inclusion of the B atom as an acceptor, as described above, gave essentially the same zfs as the six-coordinate model.
(73) Use of an average value for θ = 124 ° for all three pyrazole N ligands eliminates the rhombic splitting. This gives the sign of D directly, which is negative in both models, contrary to experiment. However, the S = 1 zero-field spin Hamiltonian has energies: $[-(2/3)|D|]$, $[+(1/3)|D| - |E|]$, and $[+(1/3)|D| + |E|]$. As $|E|$ approaches $|D|/3$ (perfectly rhombic zfs), these energies become: $[-(2/3)|D|]$, 0, and $[+(2/3)|D|]$. Thus, for significantly rhombic zfs, the sign of D is not well defined, which may be the case here.
(74) Neese, F. *J. Am. Chem. Soc.* **2006**, *128*, 10213−10222.
(75) Bruno, G.; Centineo, G.; Ciliberto, E.; Bella, S. D.; Fragalà, I. *Inorg. Chem.* **1984**, *23*, 1832−1836.

(76) Brunker, T. J.; Cowley, A. R.; O'Hare, D. *Organometallics* **2002**, *21*, 3123−3138.
(77) Brunker, T. J.; Green, J. C.; O'Hare, D. *Inorg. Chem.* **2003**, *42*, 4366−4381.
(78) Neese, F. *Coord. Chem. Rev.* **2009**, *253*, 526−563.
(79) Neese, F. *Curr. Opin. Chem. Biol.* **2003**, *7*, 125−135.
(80) Duboc, C.; Ganyushin, D.; Sivalingam, K.; Collomb, M.-N.; Neese, F. *J. Phys. Chem. A* **2010**, *114*, 10750−10758.
(81) Zein, S.; Neese, F. *J. Phys. Chem. A* **2008**, *112*, 7976−7983.
(82) Similar reactions using solid potassium borohydride were unsuccessful.
(83) Bonanno, J. B.; Henry, T. P.; Wolczanski, P. T.; Pierpont, A. W.; Cundari, T. R. *Inorg. Chem.* **2007**, *46*, 1222−1232.
(84) Analogous studies on $Tp^{Ph2}FeBH_4$ by M. Mehn were limited to solid state methods; solution phase NMR indicated considerable fluxionality in the coordinated borohydride. M. Mehn, private communication.
(85) Thorvilson, K.; Desrochers, P., unpublished results for Tp*NiX: X^-, δ (ppm): I^-, +8; Br^-, −8; Cl^-, −17; NO_3^-, −25; free Tp^{*-}, −38.
(86) The κ^1 coordination mode is also possible, and might occur with high d^n counts, which should favor less BH_4^- electron donation, but has not yet been seen.
(87) The Li-B distance in $LiBH_4$ is longer (2.48 Å)[88] than the Li-B distance in Tpm*$LiBH_4$ (2.22 Å). One expects this decrease in distance because of diminished BH_4^-/BH_4^- coulombic repulsion and a focused BH_4^- approach along the $[Tpm^*Li]^+$ dipole.
(88) Soulié, J.-P.; Renaudin, G.; Černý, R.; Yvon, K. *J. Alloys Compd.* **2002**, *346*, 200−205.
(89) Zhang, B. J.; Liu, B. H. *Int. J. Hydrogen Energy* **2010**, *35*, 7288−7294.
(90) For iron with a tripodal phosphine ligand, low spin iron(II)-borohydrides resulted.[17] Overall, the accessibility in principle to Fe(II) of both high and low spin states in LFeX complexes (L = tripodal ligand, such as $PhB(CH_2PPh_2)_3^-$ or Tp^{*-}; X = various anionic ligands) make this ion a more complicated case than Ni(II).
(91) Muñoz-Molina, J. M.; Caballero, A.; Díaz-Requejo, M. M.; Trofimenko, S.; Belderraín, T. R.; Pérez, P. J. *Inorg. Chem.* **2007**, *46*, 7725−7730.
(92) Reger, D. L.; Collins, J. E.; Matthews, M. A.; Rheingold, A. L.; Liable-Sands, L. M.; Guzei, I. A. *Inorg. Chem.* **1997**, *36*, 6266−6269.
(93) Züttel, A.; Rentsch, S.; Fischer, P.; Wenger, P.; Sudan, P.; Mauron, P.; Emmenegger, C. *J. Alloys Compd.* **2003**, *356*−*357*, 515−520.
(94) Shannon, R. D. *Acta Crystallogr.* **1976**, *A32*, 751−767.

dx.doi.org/10.1021/ic201775c | *Inorg. Chem.* 2012, 51, 2793−2805